Temporal interfaces by instantaneously varying boundary conditions

Luca Stefanini,[1,*] Shixiong Yin,[2,3] Davide Ramaccia,[1,†] Andrea Alù,[2,3,4] Alessandro Toscano,[1] and Filiberto Bilotti[1]

[1]*"Roma Tre" University, Via Vito Volterra 62, 00146 Rome, Italy*

[2]*Photonics Initiative, Advanced Science Research Center, New York, New York 10031, USA*

[3]*City College, City University of New York, New York, New York 10031, USA*

[4]*Physics Program, Graduate Center, City University of New York, New York, New York 10016, USA*

(Received 17 March 2022; revised 7 July 2022; accepted 26 August 2022; published 23 September 2022)

Temporal metamaterials have been recently exploited as a novel platform for conceiving several electromagnetic and optical devices based on the anomalous scattering response arising at a single change or multiple sudden changes in the material properties. However, they are difficult to implement in realistic scenarios by switching the permittivity of a material in time, and new strategies to achieve time interfaces in a feasible manner must be identified. In this paper, we investigate the possibility to realize a temporal metamaterial without acting on the material properties, but rather on the effective refractive index and wave impedance perceived by the wave during the propagation in an empty guiding structure by varying the boundaries in time. We demonstrate analytically and through numerical experiments that suddenly changing the structural dispersion of a parallel-plate waveguide by varying boundary conditions will induce an effective temporal interface. The proposed concept can be extended to temporally controlled metasurfaces, opening an easier path to the design and realization of novel devices based on time-varying metamaterials at microwave and optical frequencies.

DOI: 10.1103/PhysRevB.106.094312

I. INTRODUCTION

Temporal metamaterials are artificial electromagnetic materials whose effective properties vary over time. In the case of abrupt changes of the material properties, the propagating wave experiences a scattering process somewhat analogous to the one happening at the spatial interface between two different media, realizing the temporal counterpart of a spatial discontinuity. This configuration is referred to as a *temporal interface* and is characterized by the generation of a backward and a forward wave, whose amplitudes and frequencies are related to the jump of the refractive index and wave impedance between the two media, i.e., before and after the changing of medium properties [1,2]. The possibility to control the scattering by also using the time dimension has drawn significant attention in recent years [3–6]. Dual to spatially engineered materials, tailoring the material electromagnetic properties in time enables plenty of intriguing wave phenomena [7], e.g., inverse prism [8], temporal aiming [9], synthesis of effective media [10,11], temporal parity-time symmetry [12], and temporal Brewster angle [13], as well as novel devices in the time domain, e.g., antireflection coatings [14,15], temporal Fabry-Pérot cavities [16], photonic time crystals [17], and broadband absorbers [18–20]. Proposals on how to realize a temporal interface for electromagnetic waves have been issued in transmission line structures [19] and experimentally demonstrated in plasmas [21] and graphene [22] where the bulk material properties were suddenly modified. However, all the proposed techniques so far are difficult to implement in realistic scenarios, requiring changing instantaneously the properties of the whole medium where the propagation is taking place. Recently, Miyamaru *et al.* [23] have experimentally observed that a frequency shift is achieved when a laser pulse changes the carrier density of a dielectric layer where an electromagnetic wave is propagating. The change in the surface properties induces a scattering process, such as, the one observed at a temporal interface. The feasibility of temporal metamaterials is currently limited by the low implementation strategies that overcome the requirement to change the properties of the whole medium where the propagation is taking place. Novel approaches for exploiting the anomalous scattering by temporal discontinuities must be identified.

In this paper, we investigate the possibility to realize a temporal interface without acting on the actual material properties, but rather on the effective ones. Quantities, such as, the effective refractive index and effective wave impedance are typically used for describing the propagation characteristics within a guiding system, analogous to the wave propagation in an unbounded medium with the same effective material properties. Here, we consider an empty parallel-plate waveguide (PPWG) whose boundaries are suddenly changed in time to induce an effective temporal interface. Such an approach allows relaxing the steplike modulation in time of the bulk properties of the filling material and using the change in the bounding surfaces as the degree of freedom. Moreover, parallel-plate guiding systems have been already demonstrated to be an effective strategy to achieve artificial materials with negative and near-zero permittivity [24], which realizes a good platform to investigate the wave dynamics of time switching in metamaterials. In Fig. 1, we illustrate two possible strategies for enabling boundary-induced interfaces within a guiding structure: (i) changing the properties of

*To whom correspondence should be addressed: luca.stefanini@uniroma3.it

†davide.ramaccia@uniroma3.it

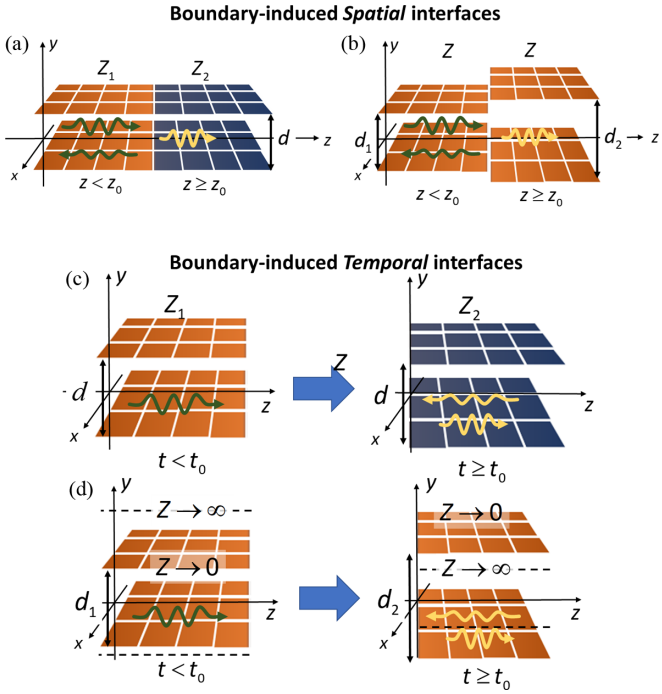

FIG. 1. Graphical illustration of the wave propagation discontinuities induced by the boundaries in a guiding structure: (a) spatial and (c) temporal interfaces induced by a change in the bounding surface impedance; (b) spatial and (d) temporal interfaces induced by a change in the separation between waveguide plates. The apparent change in separation is obtained by altering the surface impedance of two set of plates positioned at $\pm d_1/2$ and $\pm d_2/2$.

the bounding surfaces of the waveguide, represented by the arbitrary surface impedance Z [Figs. 1(a) and 1(c)]; or (ii) changing the distance between two surfaces with $Z = 0$, i.e., ideal metallic plates [Figs. 1(b) and 1(d)]. The former represents an interesting strategy for actual implementation of the boundary-induced interfaces, exploiting the recent progress in engineering the properties of metasurfaces. For example, Fig. 1(a) shows the case of two waveguides bounded by different metasurfaces realizing a spatial interface, and Fig. 1(c) shows its temporal counterpart where the surface properties are instantaneously changed over time, switching from Z_1 to Z_2 at $t = t_0$ [25–29]. This ensures the continuity of the fields across the temporal interface, being only the boundaries modified. The analysis of this configuration can be performed starting from the derivation of the eigenmodes of a metasurface-bounded waveguide for a given pair of metasurfaces as derived recently by Ma *et al.* in Ref. [30]. However, the latter strategy explores the physical process triggered by an abrupt modification of the boundary conditions over time in a more familiar manner, allowing to catch all the interesting features of a temporal interface induced through the variation of the boundary conditions more easily. At the instant $t = t_0$ the ideal metallic plates located at $d = d_1$ in Fig. 1(d) are assumed to change suddenly their conductivity from infinity to zero and, simultaneously a new pair of metallic plates located at $d = d_2$ switches their conductivity from zero to infinity. This is different than mechanically moving the plates instantaneously from d_1 to d_2, enabling a closer emulation of a sudden change in the effective refractive index perceived by the guided wave, and relaxing the modeling challenges involved in considering a continuous movement of the metallic plates [31–34]. Indeed, it is expected that the effective refractive index perceived by the wave changes abruptly in time after changing the waveguide geometry, preserving the momentum, and maintaining the spatial distribution of fields across the time interface [1,2,15].

The paper is organized as follows. In Sec. II, we first analytically derive the frequency conversion induced by the temporal interface as a function of the jump of the effective refractive index perceived by the wave before and after the boundary induced temporal interface, strongly related to the change in the interplate distance; then, by imposing the continuity of the fields across the temporal interface, we derive the scattering coefficients for the forward and backward propagating modes for TE modes. Section III is dedicated to the numerical experiments and to their comparison with the analytical results. Finally, in Sec. IV, some conclusions are drawn.

II. ANALYSIS OF BOUNDARY-INDUCED TEMPORAL INTERFACE

The scattering arising at an interface between two different media is a basic phenomenon in optics and electromagnetics. It takes place not only in presence of an actual change of the medium parameters, i.e., refractive index and wave impedance, but also at the terminals between two different waveguides [see Fig. 1(b)] as described by the well-established guided wave theory [35]. This allows extending the concept of *interface* to any spatial or temporal locus where the conservation of the wave quantities, i.e., electric and magnetic fields is not satisfied anymore. In this framework, two different waveguides support two separate sets of eigenmodes, and the matching of the mentioned quantities at the discontinuity location z_0 can be achieved only through the generation of a reflected (backward-propagating) and transmitted (forward-propagating) wave. Figure 1(d) illustrates the same abrupt change in the waveguide dimensions but in the time domain. Before the switching time $t = t_0$, the propagating mode is defined by the excitation frequency $\omega_1 = 2\pi f_1$, the waveguide dimension d_1, and the electromagnetic properties of the filling medium. At the switching time $t = t_0$, the conductivity of the metallic plates is abruptly changed to zero, and two new ideal metallic plates appear keeping the same symmetry, but now separated by d_2. This leads to a mismatch between the actual propagating mode and the ones supported by the waveguide in the new configuration. However, the scattering process at a temporal interface is deeply different with respect to the one observed at a spatial interface. In the following, we describe the considered scenario based on a parallel plate waveguide where the temporal interface induced by the boundaries is realized. The scattering problem at the interface is analytically described, showing that, in addition to the expected forward and backward scattered fields, an electrostatic field is excited such that the continuity of the total electromagnetic field is conserved across the interface.

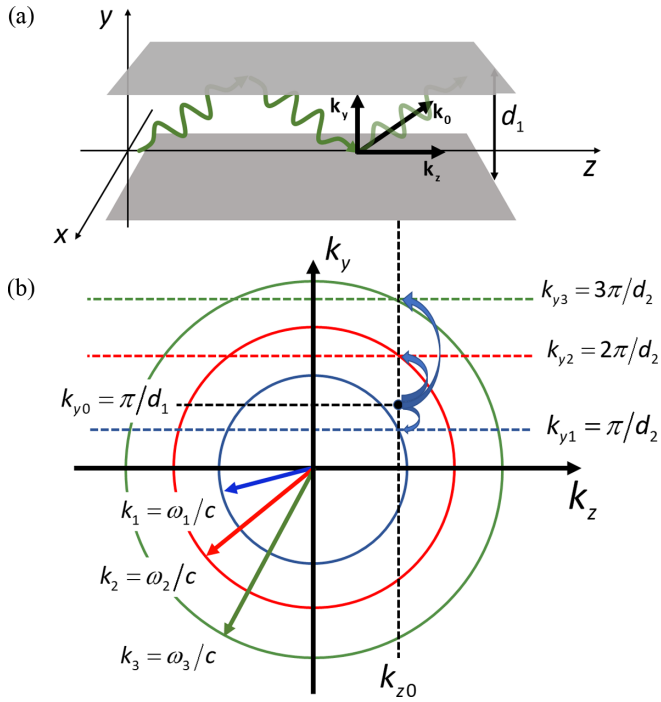

FIG. 2. (a) Representation of the propagation quantities of the modes within a parallel-plate waveguide of dimension d. (b) Dispersion diagram of the excited modes supported by the waveguide after a temporal discontinuity induced by a sudden change in the waveguide dimensions from $d = d_1$ to $d = d_2$.

A. Frequency conversion induced by boundary-induced temporal interface

Let us consider an infinitely extended PPWG consisting of two metallic plates separated by a distance d in the y direction and supporting the propagation of a z-directed wave as shown in Fig. 2(a). The waveguide is filled with vacuum ($n = 1$). The propagation of the fundamental transverse electromagnetic (TEM) mode is always supported at any frequency, whereas the TE and TM modes are supported past the corresponding cutoff frequencies, dictated by the electrical dimension d/λ, and their effective guided indices depend on the waveguide thickness d. The TEM mode, instead, always travels with the same phase velocity along the waveguide, regardless of the distance d, hence, the temporal discontinuity does not impart any change to its effective refractive index. We focus, therefore, on the excitation of TE modes. In addition, provided that our boundary modification preserves certain symmetries, TE/TM modes remain orthogonal to each other, allowing us to consider only one of the two sets. We analyze the scattering process at a boundary-induced temporal interface for a propagating TE mode. A guided wave in a PPWG described by any TE mode has always zero electric field at the metallic plate locations, ensuring zero charge accumulation on them. This allows satisfying the temporal boundary conditions for the **D** field, which must be continuous over the entire domain to mimic the switching of permittivity in an unbonded medium.

As shown in Fig. 2(a), the TE_1 mode is propagating within a PPWG. The propagation vector $\mathbf{k}_z$ is the projection along the z axis of the filling medium wave-vector $\mathbf{k}_0$, whose magnitude is $k_z = \sqrt{k_0^2 - k_y^2}$, where $k_0 = \omega/c = 2\pi/\lambda$ is the magnitude of wave number, and $k_y = \pi/d$ is the transverse wavenumber imposed by the waveguide dimensions.

In this scenario, the effective refractive index perceived by the guided mode is [36] as follows:

$$n_{\text{eff}} = \sqrt{1 - (k_y/k_0)^2} = \sqrt{1 - (\lambda/2d)^2}, \tag{1}$$

and its phase velocity is $v_p = \omega/k_z = \omega\sqrt{k_0^2 - (\pi/d)^2}$.

Here, we analyze the frequency conversion expected by an abrupt change in the waveguide dimension, which, in turn, modifies the effective medium perceived by the propagating mode. Figure 2(b) reports the dispersion diagram at the temporal interface [Fig. 1(d)], where we can identify the excited modes in the parallel plate waveguide. Before the switching time t_0, the fundamental TE_1 mode propagates with a propagation wave-number k_{z0} and a transverse wave-number k_{y0}, represented by the dashed black lines in Fig. 2(b).

At the temporal discontinuity $t = t_0$, the original propagating mode TE_1 perceives an instantaneous change in the effective refractive index from $n_{\text{eff}}(d_1)$ to $n_{\text{eff}}(d_2)$, which induces the instantaneous change in the temporal frequency through the scaling time-dilation factor ξ [7,15],

$$\omega_1 = \xi\omega_0, \quad \text{where } \xi = \frac{n_{\text{eff}}(d_1)}{n_{\text{eff}}(d_2)} = \sqrt{\frac{1 - (k_{y0}/k_0)^2}{1 - (k_{y1}/k_1)^2}}, \tag{2}$$

and the generation of a backward and a forward scattered wave, whose relative amplitudes with respect to the original mode will be derived in the next section (Sec. II B).

Here, we focus our attention on the temporal and spatial wave quantities across the interface represented on the dispersion diagram in Fig. 2(b). A temporal interface preserves the propagating wavelength λ [1], which is directly related to the propagating wave-vector k_z. In this scenario, in the same manner as a frequency source is represented by a circle in the dispersion diagram, the existing field acts as a wavelength source and is represented by the vertical black dashed line in Fig. 2(b). Therefore, in the new waveguide we have excited not only the first TE_1 mode, but also all the TE modes defined by the transverse wave-numbers $k_{ym} = m\pi/d_2$ with $m = 1, 2, 3, \ldots$, and the same original propagation wave-number $k_z = k_{z0}$ [36]. In Fig. 2(b), the circles crossing the points of intersection between k_{z0} and k_{ym} represent the wave-vectors k_m of the new modes propagating in the waveguide, each of which has a different frequency $\omega_m = ck_m$. By imposing the continuity of the propagating wave-number $k_{z0} = k_{zm}$, we analytically derive the new frequencies after the boundary-induced temporal interface,

$$\omega_m = \omega_0\sqrt{1 - \frac{k_{y0}^2 - k_{ym}^2}{k_0^2}}, \quad m = 1, 2, 3, \ldots. \tag{3}$$

B. Forward and backward scattering parameters

In this section, we focus our attention on the scattering process taking place at the boundary-induced temporal interface within a parallel plate waveguide and the analytical derivation of the amplitudes of the scattered fields in backward

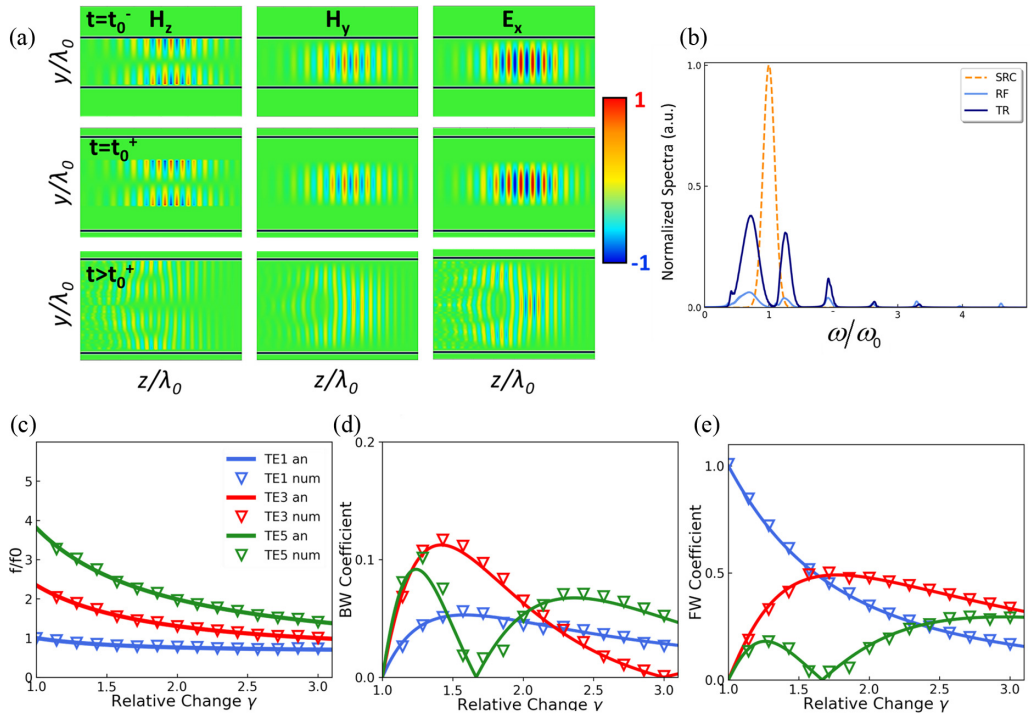

FIG. 3. (a) Snapshot in time of the—fields map within a PPWG with a boundary induced temporal interface at $t = t_0$. (b) Normalized spectra of the incident, reflected, and transmitted field at a temporal interface induced by a changing in the waveguide dimensions from d_1 to $2d_1$. (c)–(e) Comparison between analytical and numerical results for the frequencies (c), reflection coefficients (d), and transmission coefficients (e) of the excited modes after the boundary induced temporal interface as a function of the ratio $\gamma = d_2/d_1$ between the final and the initial waveguide dimension. The legend for (c)–(e) is reported in (c).

and forward directions after the interface. The most important relationship to be conserved at the interface is the continuity on the induction fields **B** and **D** [1]. In our scenario, being the bulk medium always vacuum, the condition on **B**/**D** relaxes on **H**/**E** as follows for the TE mode configuration under analysis:

$$\begin{aligned} H_z(y,z)^{t_0^-} &= H_z(y,z)^{t_0^+}, \\ H_y(y,z)^{t_0^-} &= H_y(y,z)^{t_0^+}, \\ E_x(y,z)^{t_0^-} &= E_x(y,z)^{t_0^+}. \end{aligned} \tag{4}$$

In Fig. 3 we report the components H_z, H_y, and E_x of the propagating field just before and after the temporal interface. As discussed in Sec. II A, after the temporal interface the original mode is coupled with all the modes supported by the wider waveguide with the same propagating wave number of the original one. From the microwave theory it is known that the modes inside a PPWG consist of a complete set, in other words, every supported field configuration can be cast in reason of these bases. Hence, it is convenient to expand the fields on the right-hand side of Eq. (4) as follows:

$$\begin{aligned} H_z^{t_0^+}(y,z) &= \sum_{m=1}^{+\infty} (a_m e^{i\omega_m t} - b_m e^{-i\omega_m t}) H_{z,m}^{t_0^+}(y,z), \\ H_y^{t_0^+}(y,z) &= -\sum_{m=1}^{+\infty} (a_m e^{i\omega_m t} - b_m e^{-i\omega_m t}) H_{y,m}^{t_0^+}(y,z), \\ E_x^{t_0^+}(y,z) &= -\sum_{m=1}^{+\infty} (a_m e^{i\omega_m t} + b_m e^{-i\omega_m t}) E_{x,m}^{t_0^+}(y,z), \end{aligned} \tag{5}$$

where a_m and b_m are the scattering coefficients of the forward-propagating (at frequency $+\omega_m$), and backward-propagating (at frequency $-\omega_m$) modes. The coefficients of the series expansion can be easily retrieved using the mode-matching technique: invoking the orthogonality of the modes on the right-hand side is possible to isolate each element by multiplying for the desired mth configuration and integrate over the waveguide's section. Finally, the scattering coefficients FW_m and BW_m for the mth propagating mode are

$$\begin{aligned} a_m &= FW_m = \frac{1}{2}\frac{k_{ym}}{k_{y0}}\left(1 + \frac{\omega_0}{\omega_m}\right)\kappa_{0m}^{\cos}, \\ b_m &= BW_m = -\frac{1}{2}\frac{k_{ym}}{k_{y0}}\left(1 - \frac{\omega_0}{\omega_m}\right)\kappa_{0m}^{\cos}, \end{aligned} \tag{6}$$

where $\kappa_{0m}^{\cos}$ is the overlap integral between the initial TE_1 and the final TE_m mode. Detailed information on the derivation and definition of the quantities reported in (4)–(6) can be found in Ref. [37].

III. NUMERICAL EXAMPLES

In this section, we report the results of the full wave numerical simulations carried out by using a finite-difference time-domain (FDTD) technique. A TE_1 mode is left propagating within a parallel-plate waveguide the electromagnetic fields induced by the temporal interface due to the abrupt change in the distance between the metallic plates are evaluated in real time. In all simulations, the waveguide is excited by a narrowband Gaussian pulse at frequency ω_0 for ensuring

the finite energy within the domain during the simulation but maintaining a narrow spectrum for properly computing the scattering coefficients. Following the procedure reported in Ref. [38], the metallic plates of the waveguide have been implemented in the simulator introducing two thin regions with nonzero conductivity at the location of the metallic plates, i.e., $x = \pm d_1/2$. At the instant $t = t_0$, the conductivity is suddenly switched to zero, and two new regions with nonzero conductivity appears at $x = \pm d_2/2$.

Figure 3 reports the main numerical results and their comparison with the analytical counterparts derived in Sec. II. In detail, Fig. 3(a) shows three snapshots in time of the distribution for the H_z, H_x, and E_z field components within the guiding structure before, at, and after the instant of time $t = t_0$. As expected, just after the boundary-induced temporal interface [central frames in Fig. 3(a)], the field configuration does not change satisfying the continuity of the E-H-field at the interface as expected. For $t > t_0$ [bottom frames in Fig. 3(a)], the fields within the waveguide are a superposition of several TE modes supported by the new waveguide as demonstrated in Fig. 3(b) where the spectra of the original (orange dashed line), backward-propagating (solid light-blue line), and forward-propagating (solid blue line) are reported. The different excited modes propagating at the new frequencies ω_m are clearly shown. Figures 3(c)–3(e) compare the analytical and numerical excited frequencies, backward and forward scattering coefficients, respectively, for the first three modes excited in the new waveguide after the boundary-induced temporal interface as a function of the parameter $\gamma = d_2/d_1$. These modes receive almost all the energy carried by the original TE_1 propagating in the waveguide before the switching time t_0 due to their lower phase mismatch between the original propagating and the final supported configurations. The agreement between numerical and analytical results is very good, confirming the process illustrated in Fig. 2(b).

IV. CONCLUSIONS

In this paper, we have discussed the possibility of inducing a temporal interface by acting on the effective medium properties rather than on the actual bulk material supporting the propagation. This has been demonstrated through the relevant example consisting of a TE mode propagating within a parallel plate waveguide whose boundary conditions suddenly change: The original metallic plates change their conductivity from infinity to zero letting the guided wave to propagate in a new waveguide with larger dimensions. We have described in detail the transformation from the initial to the final field configurations and derived analytically the frequency shifts imposed by the boundary-induced temporal interfaces and the backward and forward scattering coefficients for the propagating modes after it. The analytical results have been compared to FDTD numerical results, showing a perfect agreement, and validating the expected phenomenon of temporal interface. In this paper, we have focused our attention on TE modes since they have zero electric field at the metallic plate locations, ensuring zero charge accumulation on them. This allows directly satisfying the continuity of the **D** field across the interface over the entire domain. We highlight that TM modes also perceive boundary-induced temporal interfaces, and the electrodynamic scattering parameters can be derived in a similar fashion. However, it is important to pay attention in this scenario to the normal electric-field component at the metallic plate locations, which imposes a local nonzero divergence, complicating the model. In this case, the continuity of the **D** field is satisfied only if the charges are still present after the temporal interface, instantaneously anchoring them in their location. This generates a static electric field within the waveguide and will be subject of investigation in a future work. To conclude, the result reported here can be generalized to other waveguide structures, e.g., rectangular, dielectric waveguides, and optical fibers, or to metasurface-bounded guiding structures, enabling an easier path to design and realize novel devices working at microwave and optical frequencies based on the anomalous scattering caused by temporally switched material properties.

ACKNOWLEDGMENT

This work was partially supported by the Simons Foundation and the Air Force Office of Scientific Research.

[1] F. R. Morgenthaler, Velocity modulation of electromagnetic waves, IEEE Trans. Microw. Theory Tech. **6**, 167 (1958).
[2] Y. Xiao, D. N. Maywar, and G. P. Agrawal, Reflection and transmission of electromagnetic waves at a temporal boundary, Opt. Lett. **39**, 574 (2014).
[3] C. Caloz and Z.-L. Deck-Léger, Spacetime metamaterials — part I: general concepts, IEEE Trans. Antennas Propag. **68**, 1569 (2020).
[4] C. Caloz and Z.-L. Deck-Léger, Spacetime metamaterials—part II: theory and applications, IEEE Trans. Antennas Propag. **68**, 379 (2020).
[5] N. Engheta, Metamaterials with high degrees of freedom: Space, time, and more, Nanophotonics **10**, 639 (2021).
[6] G. Castaldi, V. Pacheco-Peña, M. Moccia, N. Engheta, and V. Galdi, Exploiting space-time duality in the synthesis of impedance transformers via temporal metamaterials, Nanophotonics **10**, 3687 (2021).
[7] D. Ramaccia, A. Alù, A. Toscano, and F. Bilotti, Temporal multilayer structures for designing higher-order transfer functions using time-varying metamaterials, Appl. Phys. Lett. **118**, 101901 (2021).
[8] A. Akbarzadeh, C. Caloz, and N. Chamanara, Inverse prism based on temporal discontinuity and spatial dispersion, Opt. Lett. **43**, 3297 (2018).
[9] V. Pacheco-Peña and N. Engheta, Temporal aiming, Light Sci. Appl. **9**, 129 (2020).
[10] V. Pacheco-Peña and N. Engheta, Effective medium concept in temporal metamaterials, Nanophotonics **9**, 379 (2020).
[11] V. Pacheco-Peña and N. Engheta, Temporal metamaterials with gain and loss, arXiv:2108.01007.

[12] H. Li, S. Yin, E. Galiffi, and A. Alù, Temporal Parity-Time Symmetry for Extreme Energy Transformations, Phys. Rev. Lett. **127**, 153903 (2021).
[13] V. Pacheco-Peña and N. Engheta, Temporal equivalent of the brewster angle, Phys. Rev. B **104**, 214308 (2021).
[14] V. Pacheco-Peña and N. Engheta, Anti-reflection temporal coatings, Optica **7**, 323 (2020).
[15] D. Ramaccia, A. Toscano, and F. Bilotti, Light propagation through metamaterial temporal slabs: Reflection, refraction, and special cases, Opt. Lett. **45**, 5836 (2020).
[16] J. Zhang, W. R. Donaldson, and G. P. Agrawal, Time-domain fabry–perot resonators formed inside a dispersive medium, J. Opt. Soc. Am. B **38**, 2376 (2021).
[17] E. Lustig, M. Segev, and Y. Sharabi, Topological aspects of photonic time crystals, Optica **5**, 1390 (2018).
[18] H. Li and A. Alù, Temporal switching to extend the bandwidth of thin absorbers, Optica **8**, 24 (2021).
[19] A. Shlivinski and Y. Hadad, Beyond the Bode-Fano Bound: Wideband Impedance Matching for Short Pulses Using Temporal Switching of Transmission-Line Parameters, Phys. Rev. Lett. **121**, 204301 (2018).
[20] E. Galiffi, R. Tirole, S. Yin, H. Li, S. Vezzoli, P. A. Huidobro, M. G. Silveirinha, R. Sapienza, A. Alù, and J. B. Pendry, Photonics of time-varying media, Adv. Photon. **4**, 14002 (2022).
[21] N. Yugami, T. Niiyama, T. Higashiguchi, H. Gao, S. Sasaki, H. Ito, and Y. Nishida, Experimental observation of short-pulse upshifted frequency microwaves from a laser-created overdense plasma, Phys. Rev. E **65**, 036505 (2002).
[22] A. V. Maslov and M. I. Bakunov, Temporal scattering of a graphene plasmon by a rapid carrier density decrease, Optica **5**, 1508 (2018).
[23] F. Miyamaru, C. Mizuo, T. Nakanishi, Y. Nakata, K. Hasebe, S. Nagase, Y. Matsubara, Y. Goto, J. Pérez-Urquizo, J. Madéo, and K. M. Dani, Ultrafast Frequency-Shift Dynamics at Temporal Boundary Induced by Structural-Dispersion Switching of Waveguides, Phys. Rev. Lett. **127**, 053902 (2021).
[24] M. G. Silveirinha, A. Alù, and N. Engheta, Parallel-plate metamaterials for cloaking structures, Phys. Rev. E **75**, 036603 (2007).
[25] Z. Wu and A. Grbic, Serrodyne frequency translation using time-modulated metasurfaces, IEEE Trans. Antennas Propag. **68**, 1599 (2020).
[26] D. Ramaccia, D. L. Sounas, A. Alu, A. Toscano, and F. Bilotti, Phase-Induced frequency conversion and doppler effect with time-modulated metasurfaces, IEEE Trans. Antennas Propag. **68**, 1607 (2020).
[27] B. Liu, H. Giddens, Y. Li, Y. He, S.-W. Wong, and Y. Hao, Design and experimental demonstration of doppler cloak from spatiotemporally modulated metamaterials based on rotational doppler effect, Opt. Express **28**, 3745 (2020).
[28] L. Zhang, X. Q. Chen, S. Liu, Q. Zhang, J. Zhao, J. Y. Dai, G. D. Bai, X. Wan, Q. Cheng, G. Castaldi, V. Galdi, and T. J. Cui, Space-time-coding digital metasurfaces, Nat. Commun. **9**, 4334 (2018).
[29] J. Zhao, X. Yang, J. Y. Dai, Q. Cheng, X. Li, N. H. Qi, J. C. Ke, G. D. Bai, S. Liu, S. Jin, A. Alù, and T. J. Cui, Programmable time-domain digital-coding metasurface for non-linear harmonic manipulation and new wireless communication systems, Natl. Sci. Rev. **6**, 231 (2019).
[30] X. Ma, M. S. Mirmoosa, and S. A. Tretyakov, Parallel-Plate waveguides formed by penetrable metasurfaces, IEEE Trans. Antennas Propag. **68**, 1773 (2020).
[31] J. Cooper, Scattering of electromagnetic fields by a moving Boundary: the one-dimensional case, IEEE Trans. Antennas Propag. **28**, 791 (1980).
[32] J. Cooper, Long-Time behavior and energy growth for electromagnetic waves reflected by a moving boundary, IEEE Trans. Antennas Propag. **41**, 1365 (1993).
[33] V. V. Dodonov, A. B. Klimov, and D. E. Nikonov, Quantum phenomena in resonators with moving walls, J. Math. Phys. **34**, 2742 (1993).
[34] A. V. Dodonov and V. V. Dodonov, Dynamical casimir effect via modulated kerr or higher-order nonlinearities, Phys. Rev. A **105**, 013709 (2022).
[35] R. E. Collin and IEEE Antennas and Propagation Society, *Field Theory of Guided Waves* (IEEE Press, Piscataway, NJ, 1991).
[36] D. M. Pozar, *Microwave Engineering* (Wiley, Hoboken, NJ, 2012).
[37] See Supplemental Material at http://link.aps.org/supplemental/10.1103/PhysRevB.106.094312 for detailed analyisis of the mode-matching procedure.
[38] H. P. Langtangen and S. Linge, *Finite Difference Computing with PDEs: A Modern Software Approach*, Texts in Computational Science and Engineering Vol. 16 (Springer, Cham, 2017).